Anal. Chem. **1994**, *66*, 378–383

Activity and Spectroscopic Analysis of Concentrated Solutions of K_2S

Dharmasena Peramunage, Fardad Forouzan, and Stuart Licht*

Department of Chemistry, Clark University, Worcester, Massachusetts 01610

The determination of activity of highly concentrated sulfide solutions is important for the thermodynamic analysis of speciation. A novel "evanescent" method for solvent analysis and determination of mean solution activities is applied to measure the first activity coefficients of highly concentrated sulfide solutions. Another technique, submicrometer path length spectroscopy, provides in situ observations of the problematic alkaline sulfide equilibria in the domain of highly concentrated sulfide. Combined, these methods provide an upper bound estimate for the second acid dissociation equilibrium of hydrogen sulfide of $pK_2 > 17.3(\pm 0.1)$ and the free energy of formation for sulfide of $\Delta G°(S^{2-})_{aq} > 111(\pm 0.5)$ kJ/mol.

Recently, we have presented several novel analytical methodologies specifically suited for analysis of concentrated solutions.[1] In this paper we expand on two of these methods, using the methodologies of evanescent analysis[1e] and submicrometer path length near-UV spectroscopy[1c] to probe fundamental aqueous sulfide chemistry.

H_2S is often presented as the classic case of an aqueous diprotic acid:

$$H_2S \rightleftarrows H^+ + HS^-; \quad K_1 = a_{H^+}a_{HS^-}/a_{H_2S} \qquad (1)$$

$$HS^- \rightleftarrows H^+ + S^{2-}; \quad K_2 = a_{H^+}a_{S^{2-}}/a_{HS^-} \qquad (2)$$

The second acid dissociation constant, $K_2(H_2S)$, has been reevaluated to be approximately 5 orders of magnitude smaller[2-4] than previously thought.[5,6] Its value of $pK_2 \sim 17$ indicates that, in conventional aqueous electrolytes, hydrogen sulfide speciation is strongly limited to a single deprotonation, as described by eq 1. This is significant as $K_2(H_2S)$ establishes the aqueous free energy of formation of S^{2-}, which defines over 100 known solubility constants, electrochemical potentials, and reaction thermodynamics for the metal sulfides[7] as well as impacting on fields as diverse as environmental, food, pulp, and petroleum chemistry,[8] geology,[9] and energy studies.[10]

Small values of K_2 indicate that significant S^{2-} activities will only be found in highly alkaline, highly concentrated sulfide solutions:

$$S^{2-} + H_2O \rightleftarrows HS^- + OH^- \qquad (3)$$

$$K_{2b} = K_w/K_2 = a_{OH^-}a_{HS^-}/a_w a_{S^{2-}} = f_{\pm}[OH^-][HS^-]/a_w[S^{2-}] \qquad (4)$$

where K_w is the water equilibrium constant, a_w is the activity of water, and $f_{\pm}$ the mean solution activity coefficient.

Activity considerations dominate thermodynamic properties of concentrated alkaline hydroxide solutions, increasing effective concentrations by an additional factor of 10 or more. Uncertainty in the distribution of species in alkaline sulfide solutions led to a related uncertainty in the activity coefficients attributable to these species. All previously employed solution activities in sulfide equilibria determinations were estimated from theoretical or extrapolated activity coefficients.[2-4] Using evanescent analysis, we report the first direct measurements of solvent and solution activities in these concentrated electrolytes. This allows us to incorporate real solution activity coefficients into the determination of the degree of HS^- deprotonation.

The use of very small path length (submicron path length) UV spectroscopic absorption cells permits the investigation of sulfide speciation in solutions containing 1 order of magnitude higher sulfide concentration (6.3 M) than permitted in a previous spectroscopic investigation. Measured activities of these potassium sulfide solutions are then used to establish a lower limit for $pK_2(H_2S)$ of $pK_2 > 17.3(\pm 0.1)$.

EXPERIMENTAL SECTION

Reagents. Chemicals were of analytical quality and used as received from commercial sources. Distilled deionized water was used in solution preparation. KHS solutions were prepared by saturation of KOH solutions with H_2S, as previously described.[3] K_2S is then nominally formed upon addition of equimolar KOH. Solutions were prepared, stored, and utilized under argon to prevent solution oxidation.

Methodologies. In accordance with eqs 3 and 4 and the small value for the second acid dissociation constant, $K_2(H_2S)$, highly concentrated solutions are necessary to provide high-resolution probes of free sulfide. Conventional methodologies are not suitable to determine activities or speciation of these solutions, and two alternative methodologies, evanescent analysis and submicron path length analysis, are employed in

(1) (a) Licht, S. *Anal. Chem.* **1985**, *57*, 514–519. (b) Licht, S.; Forouzan, F.; Longo, K. *Anal. Chem.* **1990**, *62*, 1356–1360. (c) Licht, S.; Peramunage, D.; Forouzan, F.; Longo, K. *Proc.—Electrochem. Soc.* **1990**, *90–10*, 241–256. (d) Licht, S.; Longo, K.; Peramunage, D.; Forouzan, F. *J. Electroanal. Interfacial Electrochem.* **1991**, *318*, 111–129. (e) Forouzan, F.; Licht, S. *Anal. Chem.* **1992**, *64*, 2003–2005.
(2) Giggenbach, W. *Inorg. Chem.* **1971**, *10*, 1333–1338.
(3) Licht, S.; Manassen, J. *J. Electrochem. Soc.* **1987**, *134*, 918–921.
(4) Meyer, B.; Ward, K.; Koshlap, K.; Peter, L. *Inorg. Chem.* **1983**, *22*, 2345–2346.
(5) *CODATA Spec. Rep.* **1980**, *No. 8*.
(6) Rao, S. R.; Hepler, L. G. *Hydrometalurgy*, **1977**, *2*, 293–299.
(7) Licht, S. *J. Electrochem. Soc.* **1988**, *135*, 2971–2975.
(8) Light, T. S. In *Ion-Selective Electrodes*; Durst, R. A., Ed.; p 349–374, National Bureau of Standards Special Publication 314; NBS: Washington, DC, 1969.
(9) Kostov, I.; Minceva-Stefona, J. *Sulphide Minerals*; Bulgarian Academy of Sciences, E. Schweizerbart'sche Verlagsbuchandlung: Stuggart, 1982.
(10) (a) Licht, S. *Nature* **1987**, *330*, 148–151. (b) Licht, S.; Manassen, J.; Hodes, G. *Inorg. Chem.* **1986**, *25*, 2486–2489. (c) Licht, S.; Peramunage, D. *J. Electrochem. Soc.* **1993**, *140*, L4–L6.

0003-2700/94/0366-0378$04.50/0

this study. In accordance with convention, activity determination are made using molal (m) units. These units are converted to molar (M) units for consistency with spectroscopic convention.

Evanescent Activity Analysis. To measure activity in solution, in a comparison of isopiestic, emf, and cryoscopic methods, only isopiestic methods were generally applicable to concentrated ($C > 0.2$ m) electrolytes.[11] Conventional isopiestic methods utilize differences in vapor pressure and take on the order of weeks to determine solvent activity. These methods are not useful in volatile or caustic media.[12-14] Recently, we introduced an evanescent (driven evaporation) measurement of water vapor pressure which correlates solvent activity to the differential mass transport from a solution phase to a controlled gas boundary layer.[1e] In a wide variety of concentrated salt solutions, evanescent probes were demonstrated to determine solvent activity to a precision of better than 2%.

In the evanescent solvent activity apparatus, all control gases were initially dehydrated and the temperature controlled to 25.0 ± 0.3 °C. Expanded experimental details are available.[1e] Calibration curves for the method are provided in Appendix 1. The output gas flow rate, maintained at 25 cm^3/s, was controlled by valve and monitored using a conventional Fisher Scientific Precision bore Flowrator 01-150/S-51801 flowmeter. A sample of solution whose activity was to be determined was situated on a balance. For the evanescent measurements of activity, the gas was introduced over a 13.2-cm^2 surface area (~50 g) of the sample and changes of solution mass with solvent evaporation were recorded. Mass measurements were determined with a computer-interfaced Fisher XA-200 electroanalytical balance with 0.1-mg resolution. Accumulated digitized data were used to calculate differential mass and applied to the analysis of solvent activity.

Submicrometer Path Length Spectroscopic Speciation Analysis. Probes for significant activities of S^{2-} necessitate highly concentrated solutions. No systematic methodology exists for absorption spectroscopy in this concentration domain. This domain requires cell path lengths which approach or surpass dimensions similar to the wavelength of incident radiation. Hence, steps in this study include the fabrication of submicrometer path length cells, the demonstration of the ability to quantify and verify these cell path lengths, and the ability to discriminate between near lying spectral features and the linearity of Beer–Lambert absorption down to this submicrometer path length domain.

Cells of micrometer or submicrometer dimensions were fabricated by sandwiching appropriate plates (as described below) in a modified 0186-0072 Perkin Elmer cell mount. Cells were assembled in a laminar flow chamber filled with prefilled Ar. Solutions were prefiltered by injection through a syringe filter.

The 0.08 μm path length cell contained two Edmund D43,400 precision single surface flats, fused quartz windows

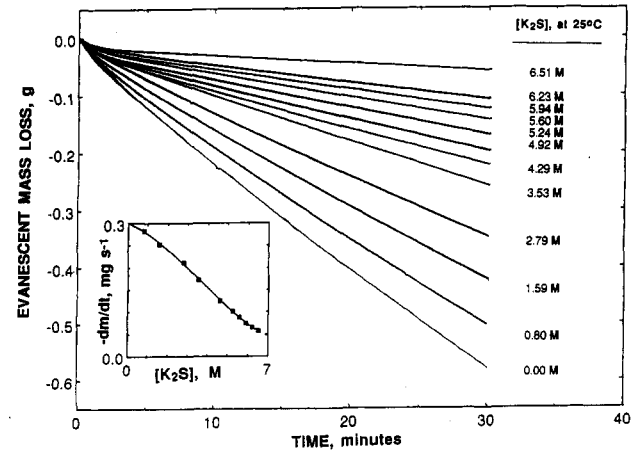

Figure 1. Evanescent mass loss of solvent from a variety of aqueous K_2S solutions. Evaporation of solvent from each K_2S solution is monitored by the mass loss of water at 25.0 °C. Figure inset: evanescent time evolved rate of mass loss, dmass/dt, as a function of K_2S molar solution concentration. $dmass_{H_2O}/dt$ is determined over 2-min increments using mass data accrued every 2.5 s over the time increment.

($^1/_{20}$ wave (31 nm) flatness, 12.7 mm diameter, 3.18 mm thickness). A 0.015 μm pore, 25 mm diameter membrane unit was used to filter both Ar and liquids. Two ESCO E210450 precision flat, fused quartz windows ($^1/_{10}$ wave (53 nm) flatness, 25.4 mm diameter, 6.35 mm thickness) were used for the 0.28 μm path length cell. In this case Ar was filtered by a 0.1 μm pore, 25.4 mm diameter membrane unit (Micron Separations DDN01025) and liquids were filtered by a 0.22-μm filter. Two ESCO Q10063 flat quartz plates, two NaCl plates without a spacer and with a 25-μm Ag wire, Alpha 00307 spacer, were used respectively for 0.56- 2.2-, and 27.7-μm cells. A 0.1 μm pore filter was used for Ar and a 0.22-μm filter was used for liquids in the last three cases. Perkin Elmer 1330 infrared spectrophotometer and Perkin Elmer Lambda 3B UV/Vis spectrophotometer were used in spectral measurements. Calibration curves for the method are provided in Appendix 2.

RESULTS AND DISCUSSION

Evanescent Sulfide Activity Analysis. Figure 1 summarizes solution mass losses, dmass/dt, from aqueous K_2S solutions at 25 °C over a wide concentration range. Potassium sulfide solutions may be nominally described as either K_2S solutions or as solutions equimolar in KOH and KHS. Molal and molar concentrations of equivalent solutions are presented in the first two columns of Table 1 and are consistent with recent density determinations.[1b] In the *evanescent* configuration described, mass loss due to the escape of H_2S_{gas} is not significant over the time domain measured. For example, as measured by precipitation in lead acetate, measured H_2S escape from 0.80 M K_2S accounts for less than 0.1% of the water vapor in the experimental configuration effluent gas. In these measurements, the high pH (solution pH values of ≥14)[1a] ensures that free H_2S activities in solution are small (≤ 10^{-7}), minimizing H_2S loss. Hence, in this study, dmass/dt is attributed entirely to solvent evaporation from the K_2S solutions.

The measured value of solvent mass loss, dmass/dt, for each of the K_2S solutions as a function of solution molarity is summarized in the inset of Figure 1. The direct conversion

(11) (a) Stokes, R. H. In *Activity Coefficients in Electrolyte Solutions*; Pytkowicz, R. M., Ed.; CRC Press: Boca Raton, FL, 1979; Vol. 1, Chapter 1. (b) Platford, R. F. *Ibid.* Chapter 3. (c) Butler, J. N. *Ibid.* Chapter 4. (d) Desnoyers, J. E. *Ibid.* Chapter 6. (e) *Ibid.* 1979; Vol. 2.
(12) Sinclair, D. A. *J. Phys. Chem.* **1933**, *37*, 495.
(13) Stokes, R. H. *J. Am. Chem. Soc.* **1947**, *69*, 1291.
(14) Williamson, A. T. *Proc. R. Soc. Edinburgh, Sect. A* **1948**, *195*, 97.

Table 1. Solvent and Mean Solution Activities of Aqueous Potassium Sulfide Solutions at 25 °C[a]

		activities		coefficients		
$[K^+]$,[b] M	$[K^+]$,[b] m	a_w	$a_\pm$ (soln)	φ	$\gamma_\pm$(activ)	$f_\pm$(activ)
0.00	0.00	1.00	0.00		1.00	1.00
0.99	1.01	0.96	0.76	0.99	0.76	0.77
1.60	1.65	0.95	1.17	0.95	0.71	0.73
3.18	3.44	0.86	3.20	1.20	0.93	1.01
5.58	6.50	0.73	8.51	1.37	1.31	1.53
7.06	8.65	0.59	18.2	1.69	2.10	2.58
9.21	12.3	0.41	47.8	2.01	3.89	5.19
10.5	14.8	0.32	79.1	2.13	5.34	7.54
11.2	16.4	0.28	103	2.18	6.29	9.20
11.9	17.9	0.23	135	2.24	7.50	11.3
12.5	19.4	0.20	170	2.30	8.75	13.6
13.0	20.9	0.17	211	2.34	10.1	16.2

[a] Potassium sulfide solutions may be nominally described either as K_2S solutions or as solutions equimolar in KOH and KHS. a_w are measured using the evanescent technique as described in the text, φ are calculated in accordance with eq 5. $\gamma_\pm$ are calculated in accordance with eq 6. $a_\pm$ is given as $\gamma_\pm[K^+, m]$. $f_\pm$ is given as $a_\pm/[K^+, M]$. [b] $[K^+] = [KOH] + [KHS]$.

of dmass/dt to a_w for K_2S is quantified in the calibration presented in the inset of Figure 6. The resulting analyzed values of a_w for aqueous K_2S solutions are presented in column 3 of Table 1. These values are compared to the known water activity of KOH solutions[15] containing the equivalent molar K^+ concentration in Figure 2.

In an aqueous solution, the variation of water activity, a_w, is described by the osmotic coefficient, φ, from

$$\varphi = -5.51 \ln a_w/(\sum_k \nu_k m_k) \quad (5)$$

where each salt k is present at molality m_k and 1 mol of the electrolyte k gives ν_k moles of ions in solution.

In accordance with Gibbs and Duhem,[11] the mean solution activity, $\gamma_\pm$, is intimately related to j (and therefore to solvent activity), and at a given concentration, $C = m$:

$$\ln \gamma_\pm(m) = \varphi(m) - 1 + \int_{C=0}^{m} [\varphi(C) - 1]C^{-1}\,dC \quad (6)$$

Solute activity may be determined from eqs 5 and 6, when solvent activities have been determined over a wide concentration range of electrolyte compositions.

Solution osmotic coefficients for sulfide solutions, φ, are presented in column 5 of Table 1 as determined from eq 5 using the evanescent water activities summarized in column 4 and the molal concentrations in column 2 of this table. Substitution of these osmotic coefficients into eq 6, and a conventional trapezoidal integration of the concentration variation of eq 6, results in the mean molal activity coefficient presented in column 6 of Table 1. Mean solution activity of these solutions, $a_\pm$, summarized in column 4, is determined as the product of this molal activity coefficient and the total concentration of KOH and KHS. As seen in this column, and analogous to concentrated potassium hydroxide solutions, extremely high solution activities are created in the high-concentration domain. Relative values of $a_\pm$ for aqueous sulfide solutions are somewhat smaller than known values for comparable KOH solutions.[15,16] In Table 1, the final column presents the molal activity coefficient, $f_\pm$, as calculated by the quotient of solution activity and molar concentration of K^+.

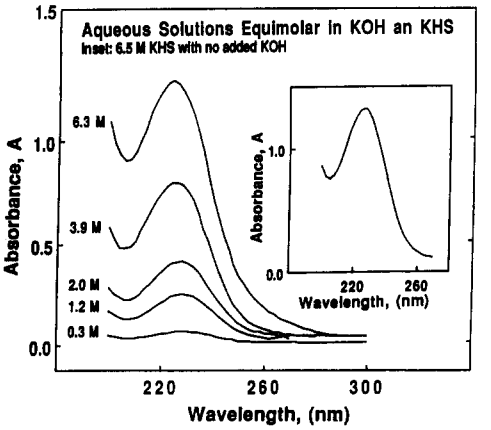

Figure 2. Water activity, a_w, of K_2S or KOH solutions at 25 °C. Values of $a_w(K_2S)$ are determined by the evanescent technique using data in Figure 1 as described in the text. Values of a_w(KOH) are from ref 16.

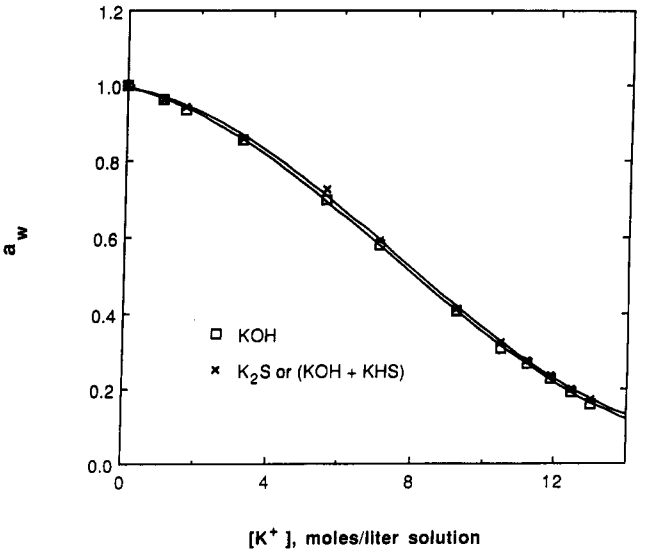

Figure 3. Near-UV spectroscopy of solutions containing equimolar aqueous KHS and KOH in a 0.28 μm path length cell at 25 °C. In repeated measurements, absorption maxima varied by up to 20%. A systematic error was observed with path length. Path length increased ~10% over the course of the measurements, attributable to alkali attack of the quartz flats. These variations are corrected for each S^{2-} concentration by normalizing absorbance to the known extinction coefficient of HS^-.[2] Shorter wavelength absorption by OH^- does not significantly affect the magnitude of the peak HS^- absorption in KHS/KOH solutions. Inset: Near-UV spectroscopy of the indicated KHS solutions at 25 °C in a 0.28 μm path length cell.

Submicrometer Path Length Sulfide Spectroscopy. The submicrometer path length cells employed consist of sandwiched optically flat quartz disks in which particulate impurities have been reduced in the ambient environment. An important spectroscopic application of the submicrometer path length domain can be for the study of equilibria in concentrated solutions of chromophores. Figure 3 presents results of 0.28 μm path length cell near-ultraviolet absorption spectroscopy of aqueous sulfide species in the very high sulfide salt concentration domain (up to 6.3 M), and Figure 4 presents results of 13 μm path length cell near-ultraviolet absorption spectroscopy in the moderately high sulfide salt concentration domain (up to 0.3 M).

(15) Akerlof, G. C.; Bender, P. *J. Am. Chem. Soc.* **1948**, *70*, 2366–2369.
(16) Harned, H. S.; Cook, M. A. *J. Am. Chem. Soc.* **1937**, *59*, 1903.
(17) Licht, S. *J. Electrochem. Soc.* **1987**, *134*, 2137–2141.

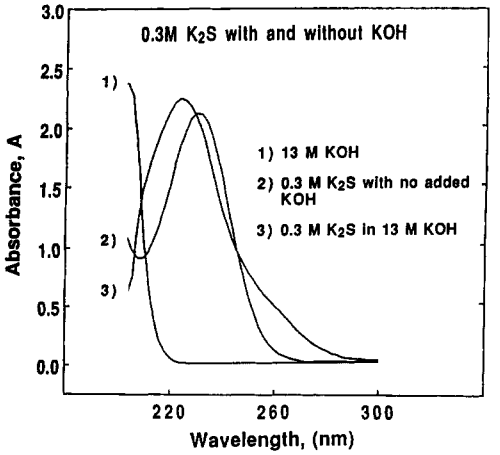

Figure 4. Near-UV spectroscopy of (1) 13 M KOH, (2) 0.3 M K_2S, or (3) 13 M KOH/0.3 M K_2S at 25 °C in a 13 μm path length cell. The curve 3 spectrum has been base line corrected for the 13 M KOH absorption spectrum.

Previous spectroscopic studies of fundamental sulfide equilibria used sodium electrolytes.[2,4] The small solubility of alkaline Na_2S compared to K_2S[17] restricts investigations of eqs 3 and 4 to low sulfide concentrations in concentrated alkaline solutions. Previous spectroscopic studies of aqueous sulfide speciation employed sodium electrolytes and therefore investigated less than 1 M added sulfide, compared to over 6 M sulfide (as K_2S) in this study. In high-concentration hydroxide electrolytes, (13 M KOH) containing low (0.3 M) concentrations of sulfide, we can reproduce the small 250-nm absorption attributed to S^{2-} previously observed[2] as a shoulder on the dominant 230-nm HS^- absorption (Figure 4). We observe an additional small shoulder at 210 nm.

Also of interest is exploration of the speciation in sulfide solutions containing the highest driving force for creation of free sulfide concentrations. In accordance with eq 4, this is attained for fixed ionic strength medium near the solubility limit of HS^- and OH^-:

$$[S^{2-}] = (K_2 f_{\pm}/K_w a_w)[OH^-][HS^-] \quad (7)$$

A 13 M KOH solution can be replaced with a similar 13 M K^+ solution, but containing 6.5 M in KOH and 6.5 M in KHS. In accordance with eq 3, this solution may be equivalently described as 6.5 M in K_2S and represents a solution approximately saturated in K_2S.[17] Rinsing of the spectroscopic cells with either 13 M KOH or water leaves no spectroscopic evidence of residual sulfide minimizing the effect of chemisorption onto the cell surface. Interestingly, as seen in Figure 3, the 250-nm absorption shoulder, attributed to the observation of free sulfide for 0.3 M KHS in 13 M KOH, does not appear even in the most concentrated K_2S solution investigated (6.3 M K_2S). This does not rule out the formation of free sulfide, but rather indicates that its absorption is dominated by the 230-nm HS^- absorption peak. Rinsing of the spectroscopic cells with either 13 M KOH or water leaves no spectroscopic evidence of residual sulfide minimizing the effect of chemisorption onto the cell surface. The small 250-nm shoulder observed in 0.3 M KHS/13 M KOH may be due to the higher driving force for relative sulfide ($[S^{2-}]/[HS^-] \propto [OH^-]$), even though the driving force for absolute sulfide is lower than in 6.3 M K_2S. However, previous labeling of the 250-nm absorption shoulder as S^{2-} cannot be considered definitive. Inspection of that previous data[2] shows that the 250-nm absorption was not accompanied by a commensurate decrease in 230-nm HS^- absorption, as would be requisite to label the 250-nm shoulder as S^{2-}. We therefore use the lack of diminution of the HS^- peak to establish an experimental upper limit to S^{2-} formation.

When free sulfide is formed, eq 3 indicates that an increase in OH^- will result in dehydrolysis and decrease in HS^-. Even in the most concentrated alkaline and sulfide solutions, the observed absorption for the HS^- peak is not substantially diminished due to the presence of concentrated hydroxide. Hence, as shown by comparison of Figure 3 and the Figure 3 inset, in K_2S solutions the magnitude of HS^- absorption has a lower bound of at least 80% of the magnitude of HS^- in KHS solutions containing no added KOH. The lower bound is reproducible to within ±15% on eight repeat measurements using three different stock solutions. In these highly concentrated solutions, none of the repeat measurements indicated the presence of a 250-nm absorption shoulder.

The activity data from Table 1 allow the first determination for the deprotonation of HS^- which incorporates real solution activity coefficients. In accordance with eq 3, a solution prepared from a nominal concentration of metal sulfide, $[M_2S]$, and containing no added alkali hydroxide, may be expressed as containing a fraction, α, of the nominal M_2S existing as free sulfide, $[S^{2-}] = \alpha[M_2S]$, and a fraction of the nominal M_2S as free hydrosulfide and hydroxide, $[HS^-] = [OH^-] = (1-\alpha)[M_2S]$. Upon rearrangement of eq 4 this provides an expression for the second acid dissociation constant for hydrogen sulfide:

$$K_2 = K_w a_w \alpha/((1-\alpha)^2 f_{\pm}[M_2S]) \quad (8)$$

Using the upper limit for free HS^- of $(1-\alpha) > 0.8$ in the most concentrated (6.3 M) K_2S solutions, we establish at 25 °C an upper limit for the second acid dissociation constant in accordance with eq 8: $K_2 < (10^{-14.0})(0.17)(0.2)/((0.8 \pm 0.12)^2(16.2)(6.5)) = 5(\pm 0.8) \times 10^{-18}$; $pK_2 > 17.3(\pm 0.1)$.

Using the established value for $\Delta G°(HS^-)_{aq} = 12.05$ kJ/mol, this yields a free energy of formation for sulfide in accordance with eq 1:

$$-RT\ln(K_2) = \Delta G°(H^+)_{aq} + \Delta G°(S^{2-})_{aq} - \Delta G°(HS^-)_{aq} \quad (9)$$

and upon rearrangement $\Delta G°(S^{2-})_{aq} > 111(\pm 0.5)$ kJ/mol.

CONCLUSION

As shown for the alkaline sulfide system, certain equilibria may be best understood in highly concentrated media. We have demonstrated that submicrometer path length UV/visible IR absorption spectroscopy is suitable for these investigations and need not be interference limited. We also demonstrate that evanescent analysis is suitable for activity determination in this concentrated solution domain. Combined, these methods provide an upper bound estimate for the second acid dissolution equilibrium of hydrogen sulfide of $pK_2 > 17.3(\pm 0.1)$ and the free energy of formation for sulfide of $\Delta G°(S^{2-})_{aq} > 111(\pm 0.5)$ kJ/mol.

ACKNOWLEDGMENT

S.L. is grateful to the Carl Julius and Anna (Kranz) Carlson Chair in Chemistry, to the National Science Foundation, and to the Dreyfus Foundation for financial support of this work.

(18) Smith, D. C.; Miller, E. C. *J. Opt. Soc. Am.* **1944**, *34*, 130–134.
(19) Koeser, H. J. K. *Fresenius' Z. Anal. Chem.* **1984**, *317*, 845.

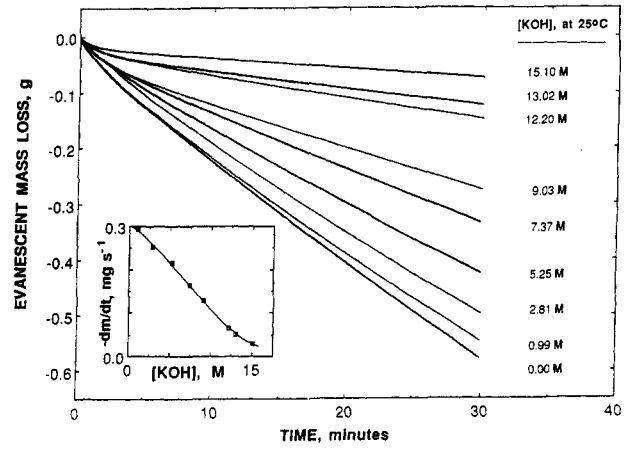

Figure 5. Evanescent mass loss of solvent from a variety of aqueous KOH solutions. Evaporation of solvent from each KOH solution into desiccated Ar is monitored by the mass loss of water at 25.0 °C, using the experimental configuration described in the text. Figure inset: evanescent time evolved rate of mass loss, dmass/dt, as a function of KOH molar solution concentration. dmass/dt is calculated from data in Figure 3 over the time increment from 500 to 1800 s.

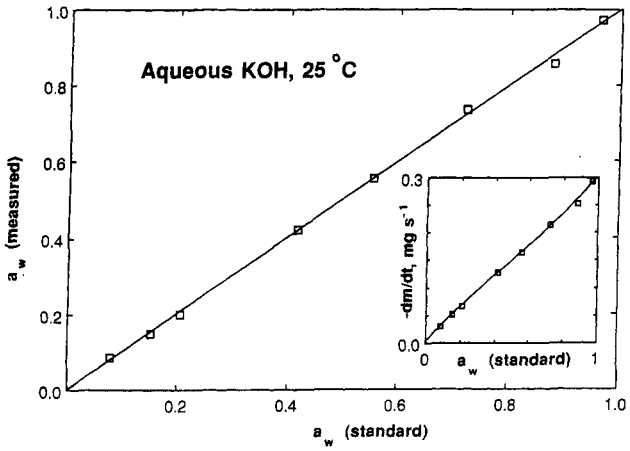

Figure 6. Comparison of known (standard) solvent activities in aqueous KOH solutions with those regenerated from evanescent measurements at 25 °C. Standard activities are from ref 11 and are in agreement with other reported values.[8,12] Values for measured activity are determined from measured evanescent values of dmass/dt using a third-order polynomial fit of dmass/dt versus a_w data summarized in the figure inset. Inset: The variation of solvent mass loss, -dmass/dt, with known water activity in aqueous KOH solutions. The curve represents a best third-order polynomial fit of the data.

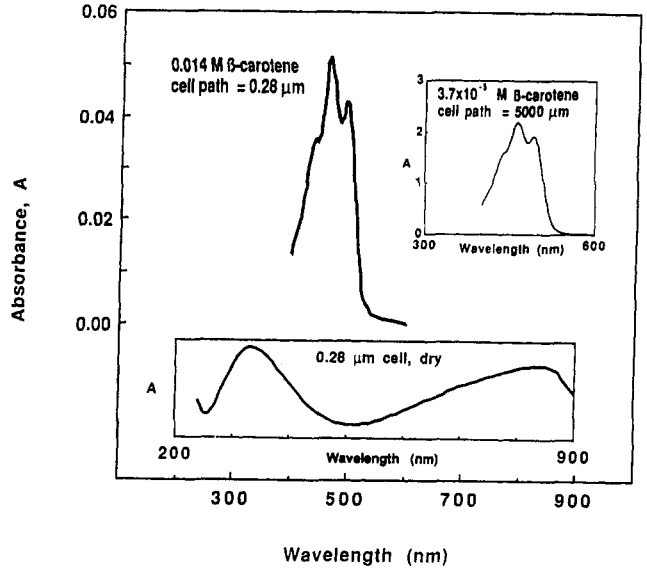

Figure 7. Absorption spectrum of benzene analytical grade solutions of β-carotene in 0.28-μm and conventional 0.5-cm (top inset) cells. Lower inset: Absorption spectrum (interference pattern) for an unfilled 0.28-μm submicrometer cell.

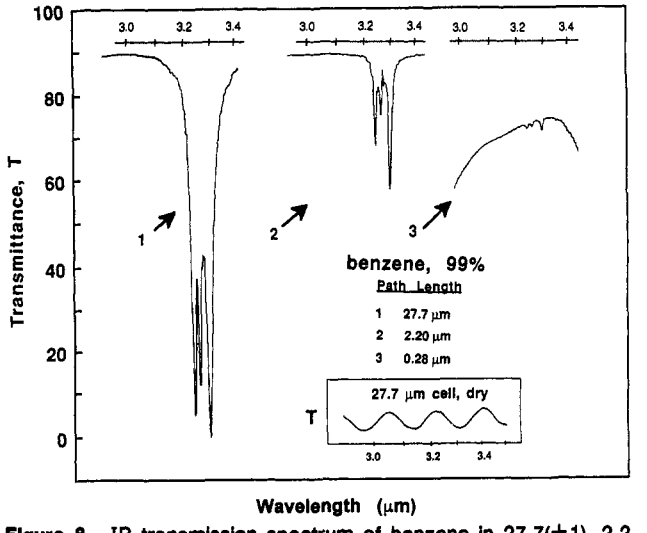

Figure 8. IR transmission spectrum of benzene in 27.7(±1), 2.2-(±0.3), and 0.28(±0.03) μm path length cells. Path lengths were determined from eq 12 and the average of several interference patterns are exemplified in the inset for a 27.7-μm cell.

APPENDIX 1

Evanescent Activity Analysis. Figure 5 presents the evanescent mass loss of a variety of concentrated aqueous KOH test solutions at 25 °C. From the data in this figure, the inset of Figure 5 summarizes the measured value of $\mathrm{dmass_{soln}}/\mathrm{d}t$ as a function of KOH solution concentration. Under a fixed gas flow and fixed cell geometry conditions, the mass transport rate of solvent across the gas/liquid interface, $\mathrm{dmass_{soln}}/\mathrm{d}t$, is related to the differential between the solution solvent activity and the solvent partial pressure in the flow gas, p_w:

$$\mathrm{dmass_{soln}}/\mathrm{d}t \propto a_w - p_w \qquad (10)$$

Solvent activities have been well characterized in KOH solutions.[15,16] The variation of these known (standard) water activities as a function of measured evanescent solvent loss, dmass/dt, is summarized in the inset of Figure 6. In accordance with eq 10, the variation of dmass/dt with a_w is highly linear to a first-order approximation, but small deviations to linearity are observed at both the low- and high-solvent activity extremes. Deviations may occur with imperfect temperature control, initial residual solvent in the carrier gas, or turbulence at the gas/liquid interface. Compensations for small deviations from linearity are incorporated by fitting a third-order polynomial for a_w. The resultant polynomial acts as a calibrating standard, an algorithm for on-line conversion of measured dmass/dt to solution activity. This method provides a measurement of the water activities in Figure 6 to an average reproducibility of 1.0% over the activity range varying from 0.86 to 0.20, and 1.6% over the full 0–1.0a_w range.

APPENDIX 2

Submicrometer Path Length Spectroscopy. Figure 7 presents the visible absorption spectrum of a high-extinction coefficient compound ($\epsilon > 10^5\ \mathrm{M^{-1}\ cm^{-1}}$), b-carotene, in cells of conventional and submicrometer path lengths. As seen in the inset of Figure 7, and as a result of the high molar

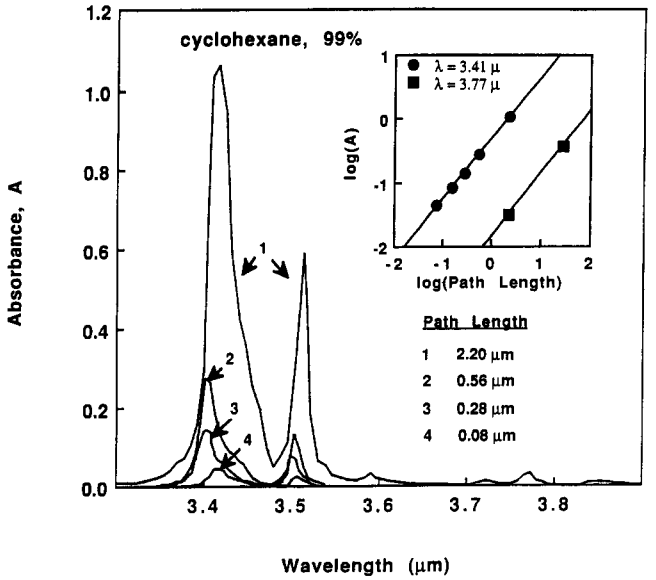

Figure 9. IR absorption spectra of cyclohexane in 2.2(±0.3), 0.56-(±0.06), 0.28(±0.03), or 0.08(±0.01) μm path length cells. Inset: Variation of the indicated cyclohexane absorption maxima from path lengths of 27.7 to 0.077 μm. Inset contains 0.162 μm path length cell data, configured as in the 0.077-μm cell, but utilizing a larger 0.10 μm pore, 25 mm diameter membrane unit. The 27.7 μm path length data exceed the absorption range at shorter wavelengths and are not included in the main figure.

absorptivity of β-carotene, spectra may be observed in a 0.5 cm path length quartz cell for β-carotene in solution of concentrations only below 5×10^{-5} M. Alternatively submicrometer path length cells will allow direct observation of substantially more concentrated solutions of β-carotene. As seen in Figure 7, the spectrum of a saturated (0.015 M) β-carotene in benzene is obtained in a cell in which the path length is reduced by 4 orders of magnitude to 0.3 μm.

The path length of the submicrometer cell utilized for the β-carotene spectroscopy has been independently determined by three techniques. First, and as seen in Figure 7, measurement of absorption within the dry cell results in a broad interference-fringe spectrum. Interference in a cell of pathlength, ℓ, results in n fringes over a wavelength range from λ_1 to λ_2:[18]

$$\ell = \frac{n\lambda_1\lambda_2}{2|\lambda_2 - \lambda_1|} \tag{11}$$

Second, cell path length is restricted by the specific flatness, f, of both of the two sandwiched optical windows and also the maximum size of particulate impurities present in the cell, p. The specific flatness is limited by either the roughness or the curvature of the optical window. Therefore, from the microscopic perspective, ℓ represents only an average distance over plates separated by surface morphology, curvature, and particulate impurities. The cell path length is limited by

$$\ell = p + 2f \tag{12}$$

Finally, ratios of ℓ may be determined by comparison of the Lambert–Beer relationship, for two cells i and j of different path lengths:

$$\ell_i = \ell_j C_j A_i / C_i A_j \tag{13}$$

Equation 11 is normally associated with infrared spectroscopy;[18] however, the submicrometer dimensions employed here necessitate calibration at near-UV/visible wavelength light. In the absence of imposed spacer materials, eq 12 recognizes that the path length arises from the extremes in microscopic surface morphology of the optical plates and impurities which separate these plates. Equation 13 assumes a constant molar absorptivity for β-carotene over the concentration range reported in Figure 7. The cell path length is determined by interference-fringe (eq 11) as 0.28 μm, by particulate limitation (eq 12) (f = 0.05 μm and p = 0.22 μm) as 0.32 μm, and by the Lambert–Beer relation (eq 13) as 0.31 μm.

Spectral discrimination of adjacent peaks is retained down to the submicrometer path length domain. We have taken advantage of the fused silica transmission window, highly transparent from 2.8 to 3.6 μm radiation, to demonstrate submicrometer path length down to the domain in which the path length is shorter than the wavelength of incident radiation. Benzene has several closely spaced C–H stretch bands in this region, and Figure 8 presents the infrared transmission spectrum of benzene in conventional and submicrometer path length cells. In each cell, including the 0.28 μm path length cell, it is seen that the C–H absorption peaks are resolved to within 6 cm^{-1} approaching the instrumental resolution. Shifts in peak position have been calculated to be significant, but are generally small (< 5 cm^{-1}) for cell window materials of various indexes of refraction.[19]

Benzene absorptivity of 3-μm light is of insufficient magnitude to discern absorption spectra in cells of less than 0.2-μm path length. Absorption spectra are investigated in cells systematically reduced to even shorter path lengths using cyclohexane with 1 order of magnitude higher absorptivity in the available transmission window ($\epsilon_{3.41\mu m}$ = 300 M^{-1} cm^{-1}) and are presented in Figure 9. In accordance with eq 11, the 0.08 (0.077) μm path length cells exhibit no discernible interference spectrum, and the optical path length was determined from eq 12 for these cells (using p = 15 nm and f = 31 nm). Figures 8 and 9 present data demonstrating the continuity of spectral shape, resolution, and position for cell path lengths substantially less than the wavelength of radiation incident upon the cell.

Figure 9 illustrates the validity of Lambert–Bouguer relations in a submicrometer path length domain. The 0.08 μm path length cell has a path length a factor of 44 shorter than the 3.41-μm wavelength of incident radiation used to measure the cyclohexane spectrum in Figure 9. No evidence of chemisorption was observed in these cells. The inset of Figure 9 presents the variation of the measured absorption from 28 to 0.08 μm cell path lengths. The data presented in the Figure 10 inset demonstrate the Lambert–Bouguer linearity of absorption amplitude with cell path length in the cell path length domain of less than $10^{-7}M$. The demonstrated linearity of absorption with path length variation and no evidence of chemisorption excludes the possibility that adsorption, chromophore orientation, or applied electric fields have been used to enhance effective light absorption. We therefore note that the results summarized in Figures 8 and 9 relate solely to bulk chromophore, and not perturbed or oriented chromophore, properties.

Received for review August 9, 1993. Accepted November 11, 1993.®

® Abstract published in *Advance ACS Abstracts*, December 15, 1993.